

Charge Transfer Efficiency in Proton Damaged CCD's

T. Hardy, *Member, IEEE*, R. Murowinski, *Member, IEEE*, and M. J. Deen, *Senior Member, IEEE*

Abstract— We have performed detailed measurements of the charge transfer efficiency (CTE) in a thinned, backside-illuminated imaging charge-coupled device (CCD). The device had been damaged in three separate sections by proton radiation typical of that which a CCD would receive in space-borne experiments, nuclear imaging, or particle detection. We examined CTE as a function of signal level, temperature, and radiation dose.

The dominant factor affecting the CTE in radiation-damaged CCD's is seen to be trapping by bulk states. We present a simple physical model for trapping as a function of transfer rate, trap concentration, and temperature. We have made calculations using this model and arrived at predictions which closely match the measured results. The CTE was also observed to have a nonlinear dependence on signal level. Using two-dimensional device simulations to examine the distribution of the charge packets in the CCD channel over a range of signal levels, we were able to explain the observed variation.

Index Terms— CCD's, charge transfer efficiency, imaging detectors, proton damage, radiation.

I. INTRODUCTION

DUE TO THEIR high sensitivity and large dynamic range, charge-coupled device (CCD) image sensors are currently finding wide use in many areas of scientific imaging, from optical astronomy to medical research. In many scientific imaging applications it is necessary to subject the detector to harmful radiative environments. Such applications include almost any space mission, X-ray crystallography, some forms of medical imaging, and energetic particle detection. The motivation for the research presented here is a radiation-intensive satellite astronomy project which requires a CCD for its attitude control system.

Light is detected by a CCD when an incoming photon generates a hole-electron pair through the photoelectric effect. The charges generated are collected into localized packets by the potential wells associated with an array of metal-oxide-semiconductor (MOS) capacitors. The amount of charge in each packet is a measure of the light intensity for

one pixel (picture element) of the sensed image. The capacitors are placed in close enough proximity that the charge on one capacitor can be transferred to the next by "spilling" it from one potential well into the other. Accomplishing this in a lossless manner is important because of the large number of transfers each packet must undergo before it reaches the output, especially with current CCD's whose array sizes have increased to millions of pixels. In these CCD's the charge packets must undergo several thousand transfers, so the efficiency must be very high. This important performance characteristic is called the charge transfer efficiency (CTE).

The CTE is the percentage of charge in a given packet which is successfully transferred from one pixel to the next and is usually represented as a single fraction, typically 0.99999 for a modern CCD. It is equivalently expressed by the charge transfer inefficiency (CTI = 1 - CTE). However, the total signal loss is not simply proportional to the amount of charge in a packet and the number of transfers it undergoes. As demonstrated in the experiments reported here, as well as our previous work [1], [2], the CTI is dependent on additional factors, including the history of charge packets transferred through a given pixel. The CTI is also extremely sensitive to damage caused by particle radiation. Much research has been done on the effects of radiation damage, and it is generally acknowledged that the increase in CTI in irradiated CCD's is due to the effects of trapping by radiation-induced trapping states. The role of traps in the CTI and their connection with particle radiation was recognized quite early [3], [4], but the increasing use of CCD's in space missions has spurred a lot of recent research in this area [5]–[10].

It has been shown, in particular, that the radiation-induced CTI is highly dependent on the temperature and the amount of time allowed for the transfer. Here we describe a simple theoretical model which explains this variation in terms of bulk trapping states and find an excellent agreement with experiment. Although a similar theoretical derivation appears in [9], this is the first time, to our knowledge, that the theory has been confirmed by experiment. It has also been shown that the CTI depends nonlinearly on the size of the charge packet, and we have been able to explain this variation using two-dimensional (2-D) simulations of the device, enhancing the work in [10], again with confirmation by experiment. A detailed knowledge of the factors, such as these which affect the CTI, will enable the user to better understand the data collected by CCD's and to optimize the operating conditions and will enable designers to improve the performance of new devices.

Manuscript received April 16, 1997; revised October 6, 1997. This work was supported in part by the Canadian Space Agency, the Dominion Astrophysical Observatory, the Natural Sciences and Engineering Research Council of Canada, and Simon Fraser University.

T. Hardy is with the School of Engineering Science, Simon Fraser University, Burnaby, B.C., V5A 1S6 Canada and the National Research Council of Canada, Herzberg Institute of Astrophysics, Victoria, B.C., V8X 4M6 Canada.

R. Murowinski is with the National Research Council of Canada, Herzberg Institute of Astrophysics, Victoria, B.C., V8X 4M6 Canada.

M. J. Deen is with the School of Engineering Science, Simon Fraser University, Burnaby, B.C., V5A 1S6 Canada (e-mail: jamal@cs.sfu.ca).

Publisher Item Identifier S 0018-9499(98)02836-6.

This paper is an extension of results first presented in [11]. Section II gives an overview of radiation damage in CCD's. Section III details a physical model of the CTI based on trapping theory. Section IV describes the experimental setup and technique. In Section V, we present the results of our experiments and in Section VI the conclusions.

II. RADIATION DAMAGE

In general, radiation causes two forms of damage to a buried channel CCD. The first is damage to the oxide and the bulk-oxide interface through ionization. This form of damage results in increased surface dark current, shifts in the flat band voltage, increased amplifier noise, and changes in linearity. The effect of increased surface dark current can be significantly alleviated by running an appropriately designed CCD in inverted or multiple-pinned phase (MPP) mode. These modes eliminate the surface dark current by inverting the surface, populating the generation centers with minority carriers, and preventing them from contributing to the generation current. Changes to the flat-band voltage can be compensated for by simply adjusting the operating voltages.

The second form of damage is caused by energetic particles such as protons or neutrons. These particles can collide with silicon atoms, displacing them from their positions in the lattice and creating vacancies within the bulk silicon. Most of the interstitial atom vacancy pairs thus created recombine and result in no permanent damage. Typically 2% of the initially generated pairs remain [12]. The vacancies which do not recombine are unstable and will migrate to more favorable positions in the lattice, often becoming trapped near impurities because of the stress these atoms cause to the lattice. The most important of the resulting defects in the CCD's we are studying appears to be the phosphorus vacancy complex (or E-center), which introduces a trapping state with an activation energy of about 0.4 eV below the conduction band [5]–[10]. However, radiation-induced traps with energies of 0.14 and 0.23 eV [4] as well as 0.12 and 0.30 eV [8] have also been reported. We found evidence for a trap at around 0.2 eV in our own measurements which suggests the presence of either an oxygen vacancy complex (A-center) or a vacancy–vacancy complex (divacancy) [13]. The trapping states created by displacement damage result in an increase in CTI and an increase in the bulk dark current. The bulk dark current may exhibit a strong spatial nonuniformity (“hot pixels”), and some pixels may show a temporal instability giving rise to random telegraph signals (RTS).

Since the *form* of the permanent displacement damage is not dependent on the energy of the incident particles, for experimental purposes we can simulate the effects of any desired energy spectrum using a monoenergetic beam by adjusting the fluence to create an equivalent number of displacements [2].

III. A SIMPLE PHYSICAL MODEL

The charge contained in the potential well beneath a CCD gate is transferred to the next and following gates by what is usually described as a simple process of phased or peristaltic

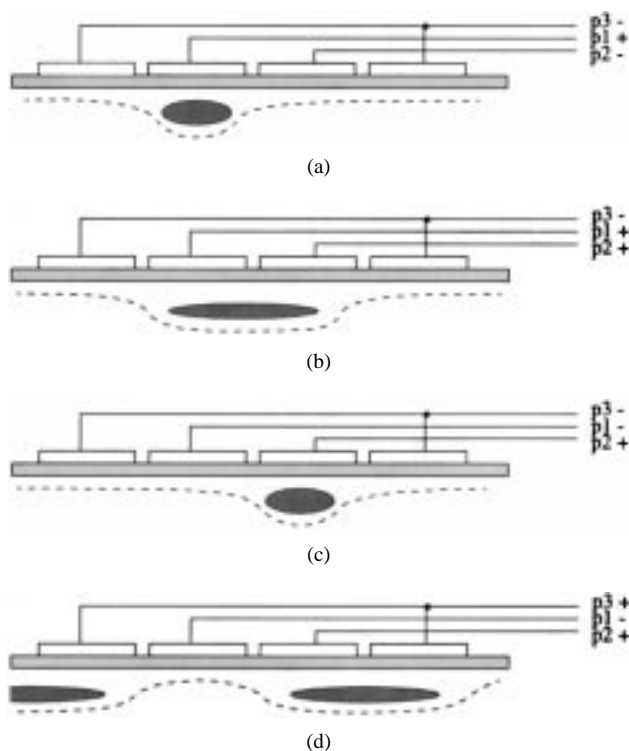


Fig. 1. Charge transfer in a three-phase CCD.

clocking. In a typical three-phase CCD, the charge is collected under one phase ($p1$ for example), which is held at a positive voltage, while the other two phases ($p2$ and $p3$) are held at negative voltages [Fig. 1(a)]. The adjacent phase in the desired direction of motion, for example $p2$, is then also made positive causing the charge packet to become distributed under $p1$ and $p2$ [Fig. 1(b)]. A short time later $p1$ is set to the negative voltage level, forcing the entire charge packet to collect under $p2$ [Fig. 1(c)]. The next transfer begins when $p3$ is set high [Fig. 1(d)] and ends with the packet under $p3$. Repeating a similar sequence with the $p3$ and $p1$ gate will move the charge packet under the next $p1$ gate, completing a one-pixel transfer for the three-phase CCD.

Charge is moved from one gate to the next by three basic mechanisms: thermal diffusion, drift due to the fringe field at the gate edges, and self-induced drift due to the mutual electrostatic repulsion between charges [15]. The efficiency of the last of these will be affected by the charge packet size, and all three will be sensitive to temperature. However, the time constants of these processes are on the order of a few nanoseconds, and at the clock rates that we used for astronomical imaging (typically $>1 \mu\text{s}$ per transfer) their effects on the CTI are negligible.

In such slow-scan applications, two mechanisms which increase CTI through charge deferral are more important: potential pockets and bulk states or traps in the silicon. Potential pockets are irregularities in the potential well shape in which signal charge can be caught during transfer. In well-designed buried-channel CCD's these pockets are minimized or eliminated, and trapping by bulk states is the more important charge-deferral mechanism. Trapping is certainly the most important effect for any CCD which has suffered bulk damage

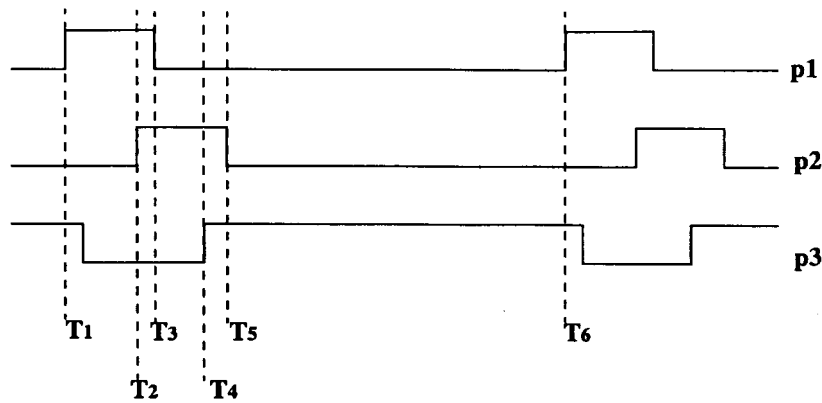


Fig. 2. Typical clocking in a three-phase CCD.

from energetic particles. A trapping state captures charges from a packet and emits them at a later time, which may be after the charge packet has been transferred to the next pixel. The charge which is “deferred” in this way is lost from the original packet and is therefore a source of CTI. The following analysis, after Kim [16], can serve as the basis of a charge deferral model resulting from bulk states. A similar analysis is given in [9].

The capture and emission time constants τ_c and τ_e [23] for the bulk states (in the case of electron traps) are

$$\tau_c = \frac{1}{\sigma_n v_{th} n_e} \quad (1)$$

$$\tau_e = \frac{e^{E_t/kT}}{\sigma_n v_{th} N_c} \quad (2)$$

where E_t is the trapping state energy level below the conduction band, σ_n is the trapping cross section, v_{th} is the thermal velocity of carriers, n_e is the density of electrons in the conduction band, and N_c is the effective density of states in the conduction band. From Sze [17]

$$v_{th} = \frac{A^* T^2}{q N_c} \quad (3)$$

where A^* is the effective Richardson constant ($252 \text{ A/cm}^2/\text{K}^2$ for n -type $\langle 100 \rangle$ Si), T is the absolute temperature, and q is the electronic charge. We can therefore express the emission time constant as a function of temperature

$$\tau_e = \frac{e^{E_t/kT}}{\sigma_n \frac{A^*}{q} T^2} \quad (4)$$

When a charge packet is present, the number of charges n_t held in bulk states within the packet volume V_s containing N_t traps per unit volume (assuming all traps are full) is given by

$$n_t = N_t V_s \quad (5)$$

When the charge packet has been removed, n_t will decrease exponentially with emission time constant τ_e so that

$$\frac{dn_t}{dt} = -\frac{n_t}{\tau_e} \quad (6)$$

Consider one gate of the typical clocking scheme of a three-phase CCD such as $p1$ of Fig. 2. We assume that the charge packet has substantially arrived under this gate at time T_1 . Traps in the volume occupied by the charge packet will be filled with time constant τ_c , and because this time constant is relatively short, we will assume the states are filled at T_1 . At time T_2 the charge packet becomes shared with $p2$ [as in Fig. 1(b)], the volume of the charge packet under $p1$ diminishes, and the traps under $p1$ begin to emit. By time T_3 the charge packet has moved on completely to $p2$. The traps under $p1$ will continue to emit until T_6 or, in the case of a sparsely illuminated CCD, until the next nonempty charge packet arrives. At that time, the states which have emitted their charges during the period since T_2 will be filled from the new packet, resulting in a charge loss from the new packet of

$$Q_{\text{trapped}} = -q N_t V_s \cdot \left(1 - e^{-(T_{\text{emit}}/\tau_e)} \right) \quad (7)$$

where T_{emit} is the total emission time from T_2 to the arrival of the new charge packet. A portion of this charge, however, is regained. Any charges emitted between T_2 and T_4 will rejoin their parent packet due to the fringe field [see Figs. 1(b) and (c)]. In fact, some of the charges emitted between T_4 and T_5 [Fig. 1(d)] will also join the parent packet, but because of uncertainty of the partition function, we will assume that the time period during which the charges can join the parent packet is $T_{\text{join}} = T_4 - T_2$. The amount of charge that is reintroduced to the packet by these emissions is

$$Q_{\text{join}} = -q N_t V_s \cdot \left(1 - e^{-(T_{\text{join}}/\tau_e)} \right) \quad (8)$$

Therefore, the net loss from a charge packet for one transfer through a $p1$ gate is

$$Q_{\text{loss}} = Q_{\text{trapped}} - Q_{\text{join}} = q N_t V_s \cdot \left(e^{-(T_{\text{emit}}/\tau_e)} - e^{-(T_{\text{join}}/\tau_e)} \right) \quad (9)$$

where T_{emit} is the emission time from the previous packet. A similar evaluation using appropriate values for T_{emit} and T_{join} can be performed for the other two phases. If more than one trap level exists, additional terms of the form of the right side of (9) can be added, using the corresponding values of τ_e and N_t .

A significant complication to the above model is the spatial distribution of the traps and the charge packets within the bulk silicon. The volume of the charge packet will vary with the number of electrons contained in it, and thus the packet will interact with a varying fraction of the traps within the pixel. The equivalent 2-D effect in surface-channel CCD's is known as the "edge effect" [18]. This three-dimensional (3-D) "shell effect" means that each shell of traps within the pixel will have a different emission period T_{emit} , which will depend on the frequency of charge packets large enough to interact with it. The traps in the outer shells, once filled by the arrival of a large charge packet, will continue to emit until a charge packet of equivalent size arrives to refill them.

A further complication is that the packet volume does not have well-defined boundaries, but rather the charge concentration falls off gradually from the center of the packet. Our earlier assumption that the capture time constant τ_c was short is not valid for small charge concentrations because τ_c is inversely proportional to the charge concentration. If the capture time constant is not short compared to the time the charge packet spends in contact with the traps, we cannot assume that all the traps are filled and (5) is no longer valid. In order to calculate the number of filled traps in the less dense shoulder regions of a charge packet, it is necessary to take this time-dependence into account. Trapping theory [10] gives the number of filled traps as

$$n_t = n_{ss} \cdot \left(1 - e^{-t/\tau_c} \cdot e^{-t/\tau_e}\right) \quad (10)$$

where t is time and n_{ss} is the number of filled traps at steady state, given by

$$n_{ss} = \frac{N_t}{1 + \tau_c/\tau_e} \quad (11)$$

and τ_c will vary across the charge packet according to (1). Therefore, the number of filled traps will depend on both the charge distribution in the packet and the amount of time t it spends in contact with the traps (the "dwell time" underneath a single gate [10]). To include this dependence in CTI calculations, the $N_t V_s$ term in (9) must be replaced by a volume integral of (10) which gives

$$Q_{\text{loss}} = q \left(\int^{V_s} n_t(x, y, z, t) dV \right) \cdot \left(e^{-(T_{\text{emit}}/\tau_e)} - e^{-(T_{\text{join}}/\tau_e)} \right). \quad (12)$$

IV. MEASUREMENTS

A. CTI Measurement Technique

A useful and simple method often used to measure the CTI of a CCD is the extended pixel edge response (EPER)

technique [5]. In this technique, the CCD is illuminated uniformly and read out in such a way as to obtain an image which extends over one or both of the edges opposite the output amplifier. The signal measured in the extended regions gives an indication of the amount of charge which has been deferred from the pixels in the imaging area of the CCD through the clocking process.

EPER is perhaps more properly considered a technique for measuring charge *deferral*, since it only gives an indirect measure of the CTI. It cannot detect losses due to charge which is completely absorbed or deferred for times much longer than the clocking periods. However, as these experiments show, EPER is still useful in examining the trapping phenomena responsible for poor CTI in radiation-damaged CCD's. The EPER technique is particularly useful in probing how the CTI changes with charge packet size, since the illumination level can be easily varied. Further advantages are that it requires no specialized equipment, and it is capable of measuring the CTI over a very wide range.

If we assume that charges are not lost during transfer, but are simply deferred by the trapping mechanism described earlier, we can see that a flat-field image such as that used for EPER will show no discernible CTI degradation. Since each charge packet is roughly the same size, the packets will interact with the same traps within the pixels, and the number of charges trapped will be the same. During each transfer, the charges emitted by the traps which do not rejoin the original packet will join the following packet and be used to refill the traps so that there is no net loss from the following packet. However, the charges captured from the last packet in a row or column will join empty packets and will not be able to interact with the traps available to the larger field packets. Therefore, the traps in the outer "shells" will not be refilled but will continue to emit their charges into subsequent packets. These packets, the "extended pixels," give a time profile of the decay of the trapped charge. Because the number of charges emitted into the extended pixels indicates the number of empty traps that would be available to capture charge from a subsequent signal packet, this number can be used to estimate the CTI.

For our results, we calculated the CTI by dividing the total amount of charge in the 40 extended pixels (the charge loss) by the average amount of charge in the last pixel of each column (the original packet size) and then dividing by the total number of single-pixel transfers involved in the read out. This gives a CTI figure equivalent to that experienced by an isolated feature in a completely dark field, which is separated from the preceding feature by 40 pixels.

B. Experimental Setup

The CCD we measured is a TK512, made by Tektronix, with 512×512 square pixels, each of $27\text{-}\mu\text{m}$ size. This device is a three-phase, thinned, backside-illuminated buried-channel device which was subjected to bulk damage by means of a 3-MeV proton beam in the University of Western Ontario's tandem accelerator in a manner similar to previous experiments [2], [19]. The imaging area and serial registers were divided into three zones which were subjected to 6.0

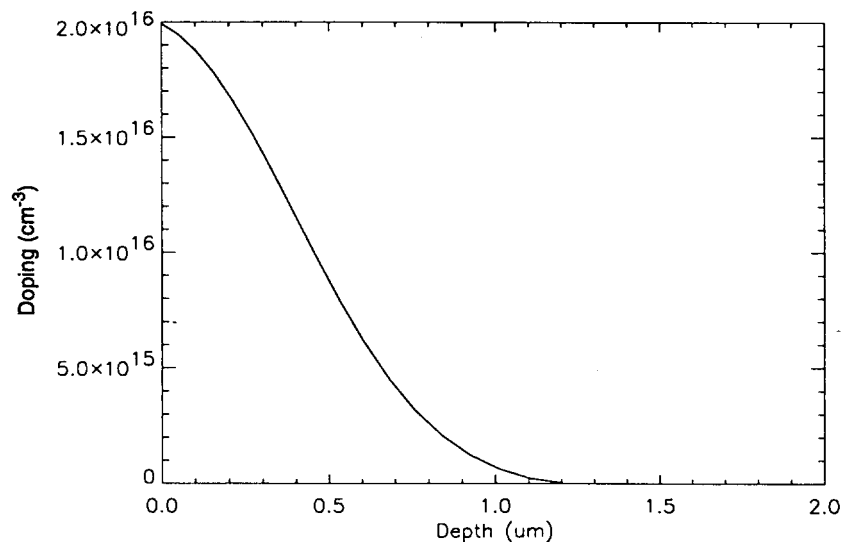


Fig. 3. Buried channel phosphorous doping profile from simulated CCD process.

$\times 10^9$ protons/cm², 1.5×10^9 protons/cm², and no radiation respectively, as measured by an event counting detector. The measured fluences are accurate to within 5%, and the beam energy is accurate to 1%. Based on estimates from TRIM software [24], the stopping distance of 3-MeV protons is much greater than the thickness of the CCD and should produce a uniform damage track all the way through the device. Our calculations indicate that the irradiations should have resulted in two damaged regions containing about 9.0×10^8 and 2.3×10^8 displacements/cm² and an undamaged control region.

The CCD is mounted in a liquid nitrogen dewar with a quartz window. A low-noise amplifier is located a short distance from the dewar to provide some gain (5–10) and to buffer the CCD output. An electronic chassis is located within one meter of the dewar, containing the clock drivers and bias supplies for the CCD. It also houses the analog signal processing chain which performs a correlated double sample with the dual slope method [19] prior to passing the signal to the 16-bit analog-to-digital converter. The electronic chassis is under the command of, and passes its data to, the data acquisition processor. Raw data are saved as disk files in the “FITS” standard [25] and are subsequently analyzed.

The temperature during the experiments is regulated with the help of a calibrated silicon diode mounted in the cold block contacting the CCD. The diode voltage drop at a constant current is used as input to a linear temperature regulator capable of depositing up to about 10 w of heat at the CCD mount. The thermal connection between the CCD mount and the 77-K station in the dewar contains a variable resistance link to allow us to further extend our experimental temperature range. A platinum resistance temperature detector (RTD) is clipped directly to the CCD package and serves to indicate the temperature of the device. By measuring the dark current, which has a well-known precise temperature dependence, we found that the RTD reading deviated from the actual device temperature by an increasing amount as the CCD was cooled (7% of the difference from room temperature). We were able to correct for this by applying a linear transformation to the RTD readings.

C. Simulations

In order to quantify the shell effect mentioned earlier, we examined the charge packet distribution within the bulk silicon using simulation software. First, we used a 2-D process simulation package, TSUPREM4 [20], to calculate the doping concentrations and create the simulation mesh for one 27- μm pixel of a three-phase buried channel CCD with an MPP implant under one of the phases (like the TK512 we measured). The simulated process started with 40 $\Omega\text{-cm}$ *p*-type silicon. The buried channel was created by an implantation of phosphorous ions (1×10^{12} cm⁻², 160 keV) and a later diffusion of 150 min at 1075 °C. The resulting doping profile is shown in Fig. 3. The channel stops were defined such that the defined channel width was 25 μm . The gate structure consisted of three separate, overlapping layers of doped polysilicon, each 9- μm wide, on a 0.1- μm oxide layer. The MPP barrier was created by a boron implant under the first gate (7×10^{11} cm⁻², 60 keV).

The simulation mesh from TSUPREM4 was then fed into a 2-D device simulation package, MEDICI [21], which iteratively solves Poisson’s equation and the charge continuity equation to calculate the potentials and charge concentrations in the device. Using MEDICI’s photogeneration feature, we were able to create a range of simulated charge packets with increasing numbers of electrons and determine the corresponding charge concentrations in the potential wells. By performing simulations of two 2-D cross sections at right angles through the device, we constructed a 3-D model of the charge concentrations and potentials. We were then able to perform the integration in (12) numerically and see the relationship between signal level and CTI due to bulk trapping.

V. RESULTS AND DISCUSSION

A. CTI as a Function of Temperature

Using the EPER technique, we measured the parallel CTI of the radiation-damaged TK512 device as a function of temperature. The CTI is also dependent on the clocking speed,

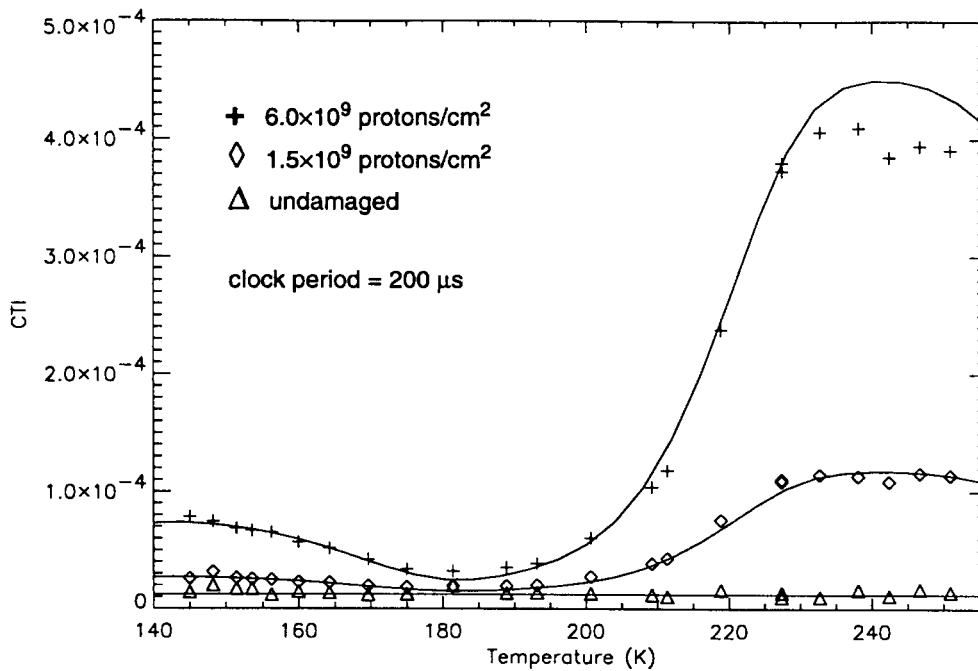


Fig. 4. Parallel CTI as a function of temperature (fast clocking). The symbols are experimental data from the three sections of the device. The lines indicate model results evaluated for a combination of the three traps in Table I.

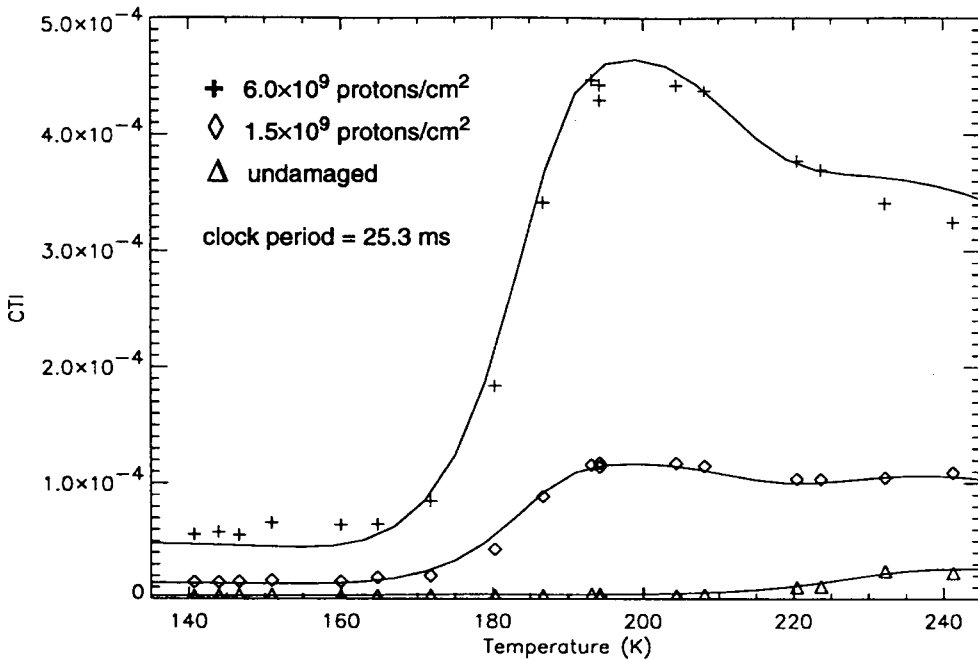


Fig. 5. Parallel CTI as a function of temperature (slow clocking). The symbols are experimental data from the three sections of the device. The lines indicate model results evaluated for a combination of the three traps in Table I.

and in many cases there are two different parallel clocking speeds to consider—a fast rate for flushing the unused parts of the array or for transferring an image into the storage region of a frame transfer device and a slower rate required when the output is being digitized. Figs. 4 and 5 show the results for these two different clock timing schemes. The three sets of data plotted in each figure indicate measurements of the three damage regions of the CCD, irradiated at various fluences as mentioned above. We note not only a general increase in CTI with an increasing amount of damage, but also that

the CTI is more strongly dependent on temperature in the damaged sections. Unfortunately, we could not get data at higher temperatures because the dark current was so high, especially in the high-radiation zone, that it was distorting the results. This distortion can be seen in the upper few temperature points of the high radiation section in Fig. 4.

Since it could be assumed that the additional CTI experienced by the TK512 from radiation damage is the result of bulk trapping, we tried to fit the trapping model described above to the data. First, the CTI in the undamaged part was

TABLE I
RADIATION-INDUCED TRAPS

Trap	E_t (eV)	σ_n (cm ²)	$N_t V_s$
A	0.21	5×10^{-16}	4.0
B	0.41	5×10^{-16}	4.0
C	0.42	6×10^{-15}	26

modeled. In Fig. 4, it was sufficient to simply model it as a constant (1.21×10^{-5}), which is shown as the lowest line. Then the model was fit to the excess CTI in the high-radiation data. The uppermost lines drawn on the graph indicates the model evaluated for a combination of three traps with the parameters given in Table I, the clock timings measured from our CCD electronics, and assuming 40 blank pixels between charge packets.

In these experiments we used the non-MPP clocking scheme shown in Fig. 2 with a clock pulse width of 96 μ s. For Fig. 4 the period of the three-phase clocking cycle was 200 μ s for the first 500 cycles, during which the serial register was simply flushed, and 22.2 ms for the final 13 cycles when the serial register was being read out between parallel transfers. The lower temperature CTI maximum in Fig. 4 is caused by Trap A and the higher maximum is a caused by the combination of Traps B and C.

In Fig. 5, we modeled the undamaged CTI as a constant (2.88×10^{-6}) plus a trapping level with $E_t = 0.48$ eV, $\sigma_n = 5 \times 10^{-16}$ cm², and $N_t V_s = 1.5$. The radiation-induced trap parameters remained the same, but the clock periods used for this figure were 25.3 ms for 490 cycles, during which the output was digitized, and 400 ms for 23 cycles when the data was being written to disk. In Fig. 5, the maxima have shifted down in temperature due to the slower clock rate and only the feature due to Traps B and C is visible.

Finally, assuming the density of trapping states is proportional to the proton dose, the model was evaluated for one-quarter of the N_t values used in the high-radiation cases, and those results were plotted as the middle lines in both figures for comparison with the low radiation data. The excellent fit indicates that the CTI increase is, in fact, proportional to the proton fluence.

When matching our model to CTI versus temperature data, it is difficult to decouple the effects of the trap energy and the trapping cross section, so we could not unambiguously determine these two parameters. We chose values which resulted in a good fit and were in line with previously published numbers. The activation energy of the lower peak seems too high to be attributable to the oxygen vacancy complex, which is generally reported to have $E_t = 0.17$ eV [13]. Therefore, we decided to try values corresponding to the divacancy, which introduces two levels that always appear in equal concentrations [4]. The parameters for Trap A and Trap B correspond to these two levels. The Trap C parameters match the published figures for the phosphorus vacancy complex, which is usually given as the dominant trap level in irradiated CCD's. Energy levels for this complex have been reported in the range 0.4–0.44 eV [5], [6], [8]–[10]. Traps B and C are not resolved in our data, and the upper

maximum could be due to a single trap at around 0.4 eV, but we introduced Trap B to see if the data were consistent with a divacancy interpretation, which it appears they are. The interaction between the trap energy and cross section makes it difficult to give representative error estimates for the data in Table I, but if we regard the cross section as fixed at a certain value, we are able to determine the trap energy to about ± 0.005 eV.

It is clear from comparing Fig. 4 with Fig. 5 that both the temperature and the clocking speed can have a significant effect on the CTI. The model we have described can be used to choose combinations of temperature and clocking speed to minimize the CTI for a radiation-damaged CCD.

B. CTI as a Function of Signal

Fig. 6 shows the simulated charge distribution for eleven different packet sizes ranging from around 100–270 000 electrons, with each subsequent packet being two to three times the size of the previous one. Each of the three plots shows the charge concentration along one axis through the center of the packet: (a) along the channel, (b) across the channel, and (c) vertically from gate to substrate. The slight asymmetry in (a) is due to the MPP implant under gate 1.

The simulated charge distributions were then processed to determine the percentage of filled traps throughout each packet. Using (10) and (11) and a dwell time of 0.1 s, we calculated the percentage of filled traps for Trap A at a temperature of 155 K. The results are shown in the three plots of Fig. 7. A dwell time of 0.1 s was used because although in a three-phase device the charge packet is present under a given phase for only about one-third of a one-pixel transfer period, in an EPER measurement there are packets in every pixel, and the time between charge packets is not long enough for the traps to empty again. Therefore, we have assumed that the *effective* dwell time is roughly the entire readout period. As it turns out, this dwell time is so long compared with the capture and emission times that the traps always reach steady state. As well, the emission time is so long that the steady-state fraction n_{ss} is always approximately one for capture time constants corresponding to electron concentrations at the limit of the accuracy of our simulation model ($\sim 10^{12}$ cm⁻³). Therefore, our data is not able to verify (10) and (11).

We then took the trap occupation data, multiplied it by the trap concentration, and performed a numerical integration over the volume of the packet to find the total number of filled traps in each packet. The discrete nature of the simulation mesh is evident in Fig. 6 and introduces an error in the number of filled traps of about 10% for the larger packets and up to 25% for the smallest packets. Finally, we inserted the number of filled traps into (12) to find the total deferred charge for comparison with experimental data.

Fig. 8 shows a plot of total deferred charge versus the packet size in electrons at a temperature of 155 K, with a logarithmic x -axis to improve the readability. The crosses represent the results of EPER measurements of deferred charge in the high-radiation section of the TK512, and the diamonds represent deferred charge in the low radiation section. The data is the total deferred charge after 500 fast parallel transfers (200 μ s

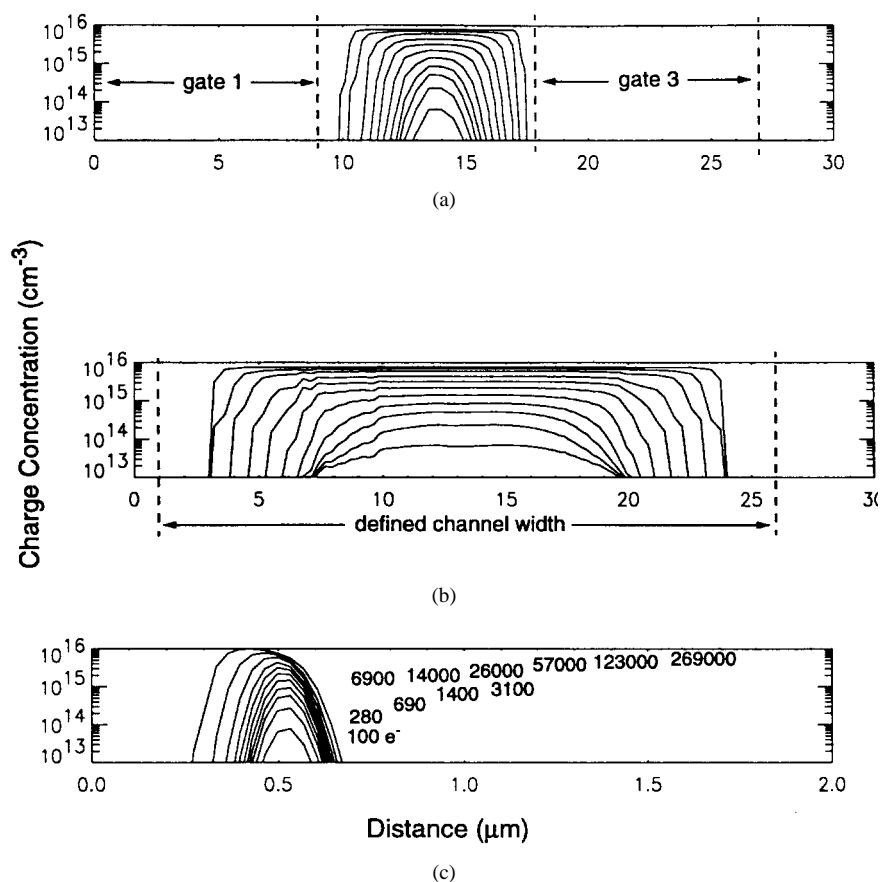


Fig. 6. Simulated charge concentration profiles under one gate of a 27- μm pixel device: (a) along channel, (b) across channel, and (c) vertically from gate to substrate, with packet sizes indicated in electrons.

per transfer). The lines represent the deferred charges calculated from the simulated charge packets, using the parameters for Trap A. The trap concentrations used for the calculations were $5.2 \times 10^{10} \text{ cm}^{-3}$ for the high-radiation section and $1.3 \times 10^{10} \text{ cm}^{-3}$ for the low-radiation section, so again we see that the trap concentrations vary linearly with proton fluence. Fig. 8 shows the corresponding estimate of CTI (DQ/s). The two lowest signal points display a poor fit due to the difficulty in accurately determining the deferred charge at such a low level. The error is magnified in Fig. 9 because of dividing by the low signal level to get the CTI.

With the stated trap parameters, the simulated results match the experimental data very well, which indicates that the nonlinear variance in CTI with signal level can indeed be explained by the variance in the packet volume and density. These results agree qualitatively with previously published results [3], [10] at low signal levels, although both of these papers show a linear dependence at high signal levels. The specifics of device fabrication, such as pixel size and channel doping, will have a large effect on the shape of the curve, so a direct comparison with these previous results is not practical.

It is well known that a CCD exhibits larger CTI for small signals, and we see here that this effect increases markedly with radiation damage. The increased CTI at small signal levels can be explained by the fact that the volume over which a charge packet is distributed is not proportional to the amount of charge contained in it. Charge packets with

small amounts of charge have a lower charge density. The bulk traps, however, have a fixed uniform density, and therefore the smaller packets interact with more traps per electron of signal. The effect in the trapping model in (12) above is to create disproportionately large CTI for smaller packets.

The importance of charge packet distribution to bulk trapping, especially for small packets, has been demonstrated clearly by the success of several researchers in using a narrow supplementary buried channel, or “notch,” to reduce the radiation-induced CTI [5], [22]. The notch is a small central section of the buried channel which has been doped higher than the rest, creating a narrow trough in the middle of the potential well. Small charge packets are constricted inside this trough, which reduces their volume and thus the number of traps they encounter. A corresponding reduction in the radiation-induced CTI is observed.

VI. CONCLUSION

We have described the temperature and signal-dependence of the CTI in proton-damaged CCD's and have presented a simple physical model to predict the CTI as a function of temperature and clocking speed for degradation due to trapping states. The model predictions are in good agreement with the experimental results. The data clearly indicates the introduction of at least two dominant bulk trapping levels as a result of proton radiation. We found the best fit to our

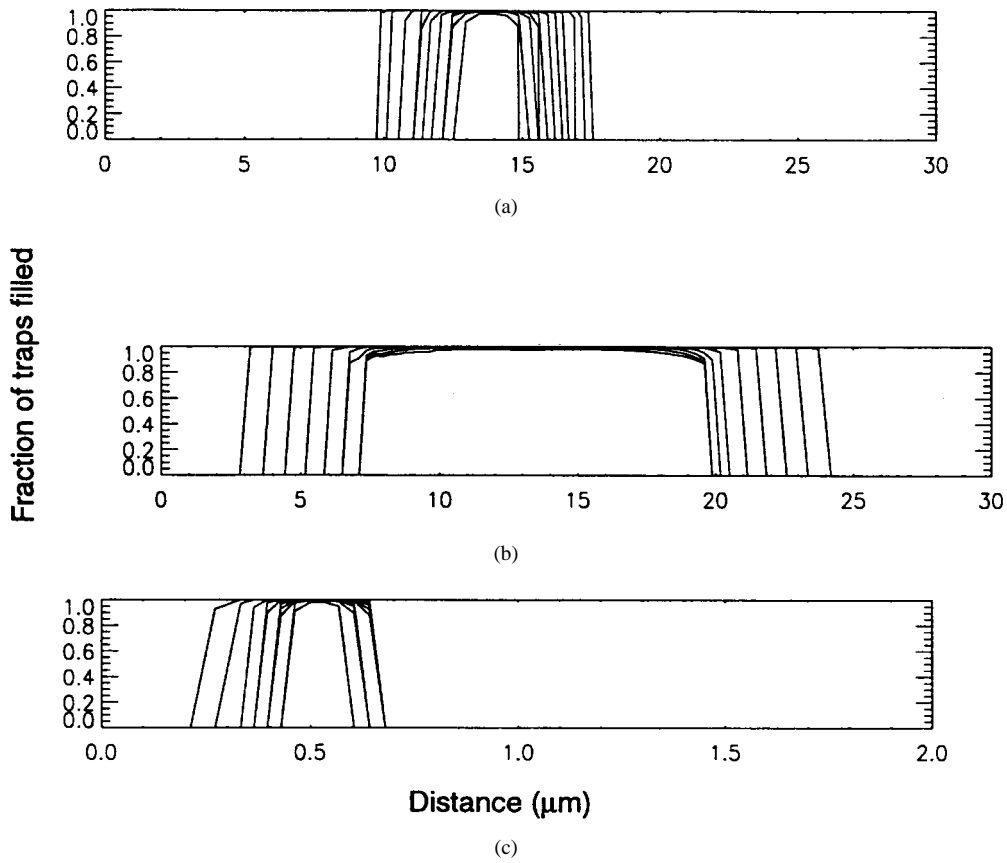


Fig. 7. Simulated filled trap profiles under one gate of a 27-mm pixel device at 155 K for a trap with $E_t = 0.21$ eV and $\sigma_n = 5 \times 10^{-16}$ cm²: (a) along channel, (b) across channel, and (c) vertically from gate to substrate.

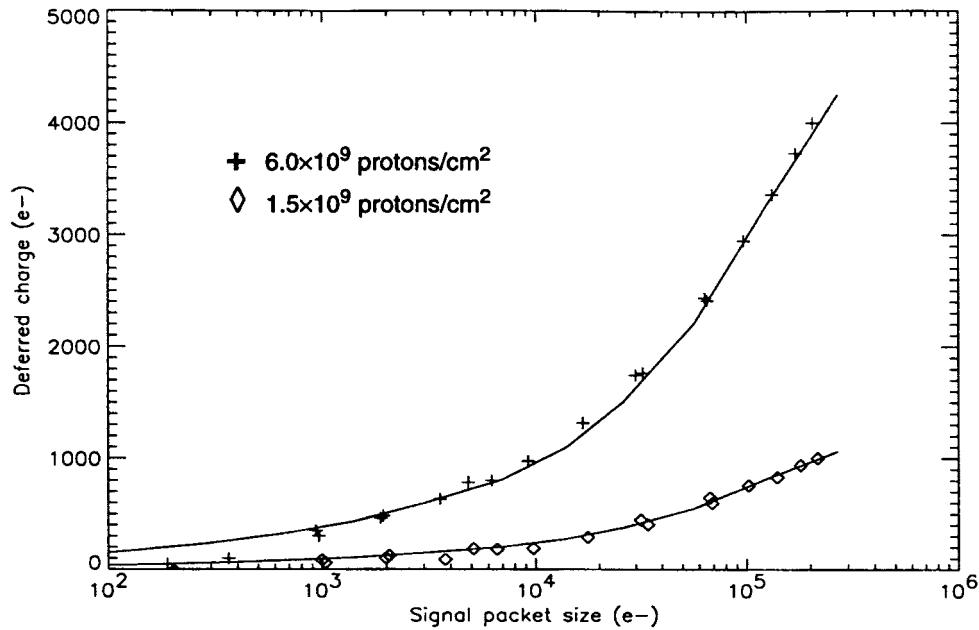


Fig. 8. Deferred charge versus charge packet size at 155 K. Symbols indicate data for the high- and low-radiation sections of the device. The lines indicate the simulated results with $E_t = 0.21$ eV, $\sigma_n = 5 \times 10^{-16}$ cm², and $N_t = 5.2 \times 10^{10}$ cm⁻³ (high) and 1.3×10^{10} cm⁻³ (low).

model with a combination of three traps and have estimated the activation energies to be about 0.21, 0.41, and 0.42 eV, respectively, with trapping cross sections of 5×10^{-16} , 5×10^{-16} and 6×10^{-15} cm². These values are in line

with published values for the divacancy and phosphorous vacancy trapping levels. The number of traps introduced appears to scale linearly with proton fluence and the ratio of concentrations of traps at the three levels is approximately

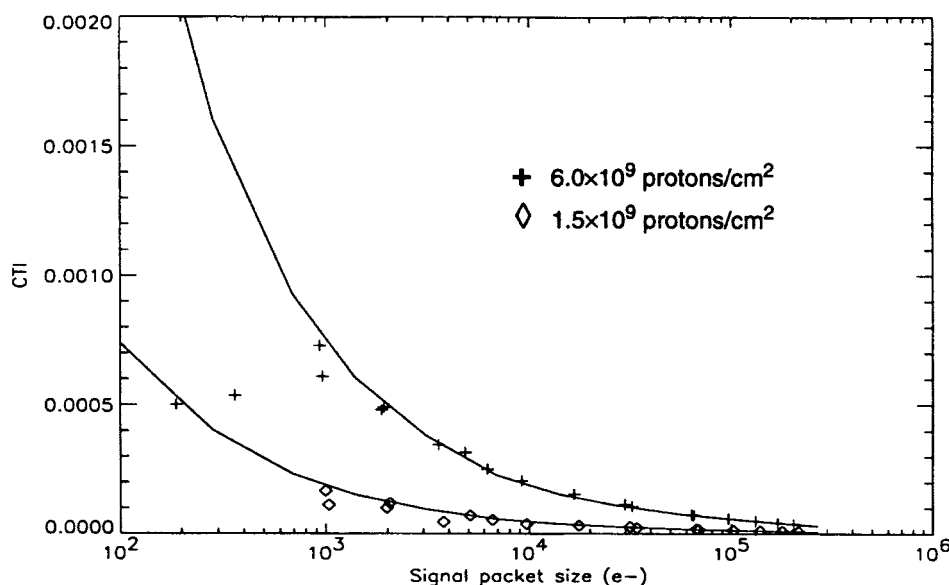


Fig. 9. CTI versus charge packet size at 155 K. Symbols indicate data for the high- and low-radiation sections of the device. The lines indicate the simulated results with $E_t = 0.21$ eV, $\sigma_n = 5 \times 10^{-16}$ cm², and $N_t = 5.2 \times 10^{10}$ cm⁻³ (high) and 1.3×10^{10} cm⁻³ (low).

1:1:6.5. After irradiation by a 3-MeV proton beam with a fluence of 6.0×10^9 protons/cm², the trap concentrations were estimated to be 5.2×10^{10} cm⁻³ for the 0.21- and 0.41-eV traps and 3.4×10^{11} cm⁻³ for the 0.42-eV trap. This corresponds to 7.8% of the expected number of bulk displacements creating 0.42-eV traps and 2.4% creating equal numbers of 0.21- and 0.41-eV traps. We have also shown, using 2-D process and device simulations, that the dependence of CTI on the signal level can be adequately explained by the variance in charge packet volume and density. The high CTI exhibited by smaller signals is due to the larger number of traps per electron of signal encountered by the smaller charge packets.

REFERENCES

- [1] R. Murowinski, M. J. Deen, and T. Hardy, "Charge transfer efficiency in low temperature charge coupled devices," in *Proc. Symp. Low Temperature Electronics and High Temperature Superconductivity*, vol. 95-9, C. Claeys, S. Raider, R. Kirschman, and W. Brown, Eds. NJ: Electrochemical Soc. Press, 1995, pp. 369-382.
- [2] R. Murowinski, G. Linzhuang, and M. J. Deen, "Effects of space radiation damage and temperature on CCD noise for the Lyman FUSE mission," in *Photonics for Space Environments, Proc. SPIE*, E. Taylor, Ed., 1993, vol. 1953, pp. 71-81.
- [3] A. Mohsen and M. Tompsett, "The effects of bulk traps on the performance of bulk channel charge-coupled devices," *IEEE Trans. Electron Devices*, vol. ED-21, pp. 701-712, 1974.
- [4] N. S. Saks, "Investigation of bulk electron traps created by fast neutron irradiation in a buried n-channel CCD," *IEEE Trans. Nucl. Sci.*, vol. NS-24, pp. 2153-2157, 1977.
- [5] J. Janesick, G. Soli, T. Elliot, and S. Collins, "The effects of proton damage on charge-coupled devices," in *Proc. SPIE*, 1991, vol. 1447, pp. 87-108.
- [6] M. S. Robbins, T. Roy, and S. Watts, "Degradation of the charge transfer efficiency of a buried channel charge coupled device due to radiation damage by a beta source," in *Proc. RADECS*, 1992, pp. 327-332.
- [7] I. Zayer, I. Chapman, D. Duncan, G. Kelly, and K. Mitchell, "Results from proton damage tests on the Michelson Doppler Imager CCD for SOHO," in *Proc. SPIE*, 1993, vol. 1900, pp. 97-107.
- [8] A. D. Holland, "The effect of bulk traps in proton irradiated EEV CCD's," *Nucl. Instrum. Methods*, vol. A326, pp. 335-343, 1993.
- [9] C. Dale, P. Marshall, B. Cummings, L. Shamey, and A. Holland, "Displacement damage effects in mixed particle environments for shielded spacecraft CCD's," *IEEE Trans. Nucl. Sci.*, vol. 40, pp. 1628-1637, 1993.
- [10] I. H. Hopkins, G. Hopkinson, and B. Johlander, "Proton-induced charge transfer degradation in CCD's for near-room temperature applications," *IEEE Trans. Nucl. Sci.*, vol. 41, pp. 1984-1991, 1994.
- [11] T. Hardy, R. Murowinski, and M. J. Deen, "Charge transfer efficiency in proton damaged CCD's," in *Proc. ESO Workshop Optical Detectors for Astronomy*, J. W. Beletic and P. Amico, Eds. New York: Kluwer, 1997.
- [12] V. A. J. Van Lint, "The physics of radiation damage in particle detectors," *Nucl. Instrum. Methods*, vol. A253, pp. 453-458, 1987.
- [13] Z. Li, H. Kraner, E. Verbitskaya, V. Eremin, A. Ivanov, M. Rattaggi, P. Rancoita, F. Rubinielli, S. Fonash, C. Dale, and P. Marshall, "Investigation of the oxygen-vacancy (A-center) defect complex profile in neutron irradiated high resistivity silicon junction particle detectors," *IEEE Trans. Nucl. Sci.*, vol. 39, pp. 1730-1738, 1992.
- [14] G. R. Hopkinson, C. J. Dale, and P. W. Marshall, "Proton effects in charge-coupled devices," *IEEE Trans. Nucl. Sci.*, vol. 43, pp. 614-627, 1996.
- [15] E. K. Banghart, J. Levine, E. Trabka, E. Nelson, and B. Burkey, "A model for charge transfer in buried channel charge-coupled devices at low temperature," *IEEE Trans. Electron Devices*, vol. 38, pp. 11620-1174, 1991.
- [16] Ch.-K. Kim, in *Charge-Coupled Devices and Systems*, M. J. Howes and D. V. Morgan, Eds. New York: Wiley, 1979, p. 57.
- [17] S. M. Sze, *Physics of Semiconductor Devices*. New York: Wiley, 1981, p. 261.
- [18] M. F. Tompsett, "The quantitative effects of interface states on the performance of charge-coupled devices," *IEEE Trans. Electron Devices*, vol. ED-20, no. 1, pp. 45-55, 1973.
- [19] R. Murowinski, G. Linzhuang, and M. J. Deen, "Effects of space radiation damage and temperature on the noise in CCD's and LDD MOS transistors," *IEEE Trans. Nucl. Sci.*, vol. 40, pp. 288-294, 1993.
- [20] TMA TSUPREM-4, *Two-Dimensional Process Simulation Program*, Version 6.1, Technology Modeling Associates, Inc., Palo Alto, CA, 1994.
- [21] TMA MEDICI, *Two-Dimensional Device Simulation Program*, Version 2.0, Technology Modeling Associates, Inc., Palo Alto, CA, 1994.
- [22] A. Holland, A. Holmes-Siedle, B. Johlander, and L. Adams, "Techniques for minimizing space proton damage in scientific charge-coupled devices," *IEEE Trans. Nucl. Sci.*, vol. 38, pp. 1663-1670, 1991.
- [23] M. J. Deen, J. I. Iowski, and P. Yang, "Low frequency noise in polysilicon-emitter bipolar junction transistors," *J. Appl. Phys.*, vol. 77, no. 12, pp. 6278-6288, June 15, 1995.
- [24] J. Ziegler, J. Biersack, and U. Littmark, *The Stopping and Range of Ions in Solids*. New York: Pergamon, 1985.
- [25] D. C. Wells, E. W. Greisen, and R. H. Harten, "FITS: A flexible image transport system," *Astronomy and Astrophys. Supplement Series*, vol. 44, pp. 363-370, 1981.